Current Assisted Memory Effect in Superconductor-Ferromagnet Bilayers: A Potential Candidate for Memristors

Hasnain Mehdi Jafri[1,2], Xingqiao Ma[1]*, Houbing Huang[2], Congpeng Zhao[1,3], Hafiz Imran Ahmad Qazi[4], Syeda Beenish Fatima Kazmi[5], Zhuhong Liu[1], Lihua Liu[1], San-Qiang Shi[6], Yang Li[7] and Long-Qing Chen[8]

[1]Department of Physics, University of Science and Technology Beijing, Beijing 100083, P. R. China

[2]Advanced Research Institute of Multidisciplinary Science, Beijing Institute of Technology, Beijing 100081, P. R. China

[3]ASIC, China Center for Information Industry Development, Beijing 100083, P. R. China

[4]Department of Engineering Physics, Tsinghua University, Beijing 100083, P. R. China

[5]College of Material Science and Engineering, Beijing Forestry University, Beijing 100083, P. R. China

[6]Department of Mechanical Engineering, Hong Kong Polytechnic University, Hung Hom, Kowloon, Hong Kong

[7]School of Engineering, University of Puerto Rico at Mayaguez, Mayaguez, PR 00681-9000, USA

[8]Department of Materials Science and Engineering, The Pennsylvania State University, University Park, Pennsylvania 16802, USA

*Email: xqma@sas.ustb.edu.cn

ABSTRSCT

Superconductivity and ferromagnetism are two very useful phenomena but rarely coexist in bulk materials. Bringing them together in artificial hybrid bilayer produces some unusual results. We designed and studied a system of superconductor-ferromagnet bilayer with a thin insulating buffer layer between them. Such a superconductor-ferromagnet bilayer with magnetostatic coupling is proposed to be used as a multibit superconductor memory device and a potential candidate for memristor. Numerical simulations were performed by using Ginzburg-Landau and Landau-Lifshitz-Gilbert models for superconductor and ferromagnet materials, which highlighted some interesting resistive memory effects in superconducting layer in the bilayer system. Vortex pattern in superconductor was observed to be

strongly coupled with ferromagnet domain structure, while their dynamics controlled by the current flowing through the superconductor. Carrier concentration, energy components and magnetization in the superconducting layer were studied as a function of applied current pulses in the superconductor layer, indicating the information storage of current pulses. Multiple resistive states were observed, pointing towards the possibility of such a device to be used as multibit data storage device.

Keywords: superconductor-ferromagnet bilayer, Ginzburg-Landau model, superconducting memories, memristors

1. INTRODUCTION

It is generally believed that in the context of the Bardeen–Cooper–Schrieffer (BCS) theory of superconductivity, conduction electrons in a metal cannot be both ferromagnetically ordered and superconducting [1]. Even when the superconductivity has been interpreted as arising from the magnetic mediation of the paired electrons, it is considered to occur in the paramagnetic phase [2]. Ferromagnetism is usually considered to be incompatible with conventional superconductivity, as it destroys the singlet correlations responsible for the pairing interaction. These characteristics do not coexist in conventional materials, but they can be brought together artificially by joining two types of materials together. In the present work, we combined ferromagnet (FM) and superconductor (SC) with an insulating buffer layer between them, prohibiting electrical coupling and allowing only magnetostatic coupling between the layers. Magnetostatic coupling arises from the interaction between ferromagnetic stray field and magnetization at vortices. Some recent reports on such hybrid systems mainly focused on the effect of magnetic domain structure on superconducting vortices with emphasis on flux pinning of superconducting vortices with magnetic nano-rod array [3], ferrite nanoparticles [4], arrays of magnetic dots [5], magnetic templates [6], magnetic dipoles[7] magnetic domain walls [8] and magnetic micro loops [9]. Electrical transport in SF bilayer system have been studied for Nb/Co[10]**,** Al/CoPd [11], NbSe2/Py [8] MoGe/Py [12, 13] and Pb/Py [14] bilayers. Where a guided vortex motion with domain wall in desired direction have been controlled by in-plane oriented external magnetic fields [8, 12-14]. Superconductor-ferromagnet (SF) bilayer system has already been studied extensively for proximity effects [15-23], domain wall superconductivity [8, 24-28], induced ferromagnetism [6, 29, 30], induced superconductivity [31, 32], transition temperature manipulation [33-35] and triplet superconductivity [36-38] to name a few. To the best of our knowledge, there are no reports of vortex structure manipulations where superconductor currents are thought to be the cause.

We observed memristive characteristics in the SF bilayer when subjected to current pulses in SC layer. As we know, the memristor is the fourth missing circuit element, defined having memresistance M as a function of charge and flux $d\varphi/dq = M$ [39]. Because of expected applications, along with their physically and industrially interesting properties, the memristor has brought about a great deal of

attention and has stimulated experimental and theoretical studies. Various observations of memristor characteristics in different devices have been reported, including self-directed channel memristor [40], Titanium dioxide memristor [41], perovskite memristors [42], layered memristors [43], ferroelectric memristors [44], carbon nanotube memristor [45], organic memristors [46, 47], spintronic memristor using spin-torque magnetization motion [30], and organic/inorganic halides [48], but still there is no widely accepted memristor model/device and search for new type of materials and structures is an open arena.

In our current research, we investigated the effect of magnetostatic coupling in a hybrid system of SF bilayer. We discussed the memristive characteristics in superconducting stripes in a certain environment variables range. By using combined Landau-Lifshitz-Gilbert equations (for FM layer) and Ginzburg-Landau Equations (for SC layer), we simulated SF bilayer separated by a thin buffer layer. Current assisted resistance memory characteristics were observed. Introduction of current pulses resulted in memory effect in SC layer, in terms of carrier concentration of superconducting layer. This effect was also cross-validated by observation of similar memory effect in energy components and SC magnetization. We propose such a system as a potential candidate for memristor and long-awaited multi-bit superconducting memory devices.

2. Numerical techniques

2.1 Landau-Lifshitz-Gilbert Equations

In order to determine equilibrium domain structure, the micromagnetic simulations were used. Micromagnetic simulation is based on the dynamic evolution of time-dependent Landau-Lifshitz-Gilbert equation [49, 50] given as:

$$\frac{\partial \boldsymbol{m}}{\partial t} = -\gamma \boldsymbol{m} \times \boldsymbol{H}_{eff} - \frac{\alpha_m}{M_s} \boldsymbol{m} \times (\boldsymbol{m} \times \boldsymbol{H}_{eff}) \quad (1)$$

where $\boldsymbol{m}$ is normalized magnetization given as $\boldsymbol{m}=\boldsymbol{M}/M_s$, where $\boldsymbol{M}=\boldsymbol{M}(m_x,m_y,m_z)$ is magnetization vector along three coordinate axes, where γ, α, and M_s is gyromagnetic ratio, damping coefficient, and saturation magnetization, respectively. The H_{eff} is effective magnetic field defined by derivative of total Gibbs free energy F_M with respect to magnetization M:

$$\boldsymbol{H}_{eff} = -\frac{1}{\mu_0} \frac{\delta F_M}{\delta \boldsymbol{M}} \quad (2)$$

where

$$F_M = F_{ex} + F_{an} + F_{dem} + F_{zee} \quad (3)$$

where F_{ex}, F_{an}, F_{dem} and F_{zee} is exchange energy, anisotropy energy, demagnetization field energy and F_{zee} is Zeeman energy, respectively, when a magnetic field is applied. Exchange energy given as:

$$F_{ex} = \frac{A}{2M_s^2}\int_V \left((\nabla M_x)^2 + (\nabla M_y)^2 + (\nabla M_z)^2\right) dV \quad (4)$$

where A is ferromagnetic exchange constant, F_{ex} keeps neighbouring magnetic moments parallel to each other. Magnetocrystalline energy is responsible for aligning magnetization along certain crystallographic directions, for uniaxial materials it could be given as:

$$F_{an} = \frac{K_u}{M_s}\int_V (1 - (\mathbf{M}\cdot\mathbf{k})^2)\, dV \quad (5)$$

where K_u is uniaxial anisotropy constant and k is unit vector in magnetocrystalline easy axis. Demagnetization energy is responsible for the formation of magnetic domains and is given as:

$$F_{dem} = -\frac{\mu_0}{2}\int_V \boldsymbol{H}_d \cdot \boldsymbol{M}\, dV \quad (6)$$

Zeeman energy rotates magnetization parallel to the magnetic field is given as:

$$F_{zee} = -\mu_0 \int_V \boldsymbol{M}\cdot\boldsymbol{B}\, dV \quad (7)$$

where **B** is the external magnetic field applied to the system.

2.2 Ginzburg Landau Theory of superconductivity

In order to study the magnetic structure in type-II superconductors, the phenomenological Ginzburg-Landau Theory was used. Time-dependent Ginzburg-Landau(TDGL) equations were developed by Gorkov and Eliashberg [51]. Our starting point is the version of equations, reported in references [52, 53]. Gibbs free energy of superconducting sample with superconducting order parameter ψ and magnetic vector potential A, given as:

$$G(\psi, \boldsymbol{A}) = \frac{1}{2m}|(\hbar\boldsymbol{\nabla} - \imath e\boldsymbol{A})\psi|^2 + \alpha|\psi|^2 + \frac{1}{2}\beta|\psi|^4 + \frac{1}{2\mu_o}|\boldsymbol{\nabla}\times\mathbf{A} - \mu_o\boldsymbol{B}|^2 \quad (8)$$

Where $\hbar = h/2\pi$, h is Plank's constant, m and e are effective mass and charge of charge carriers, α and β are phenomenological parameters depending on external factors, α is negative below the critical temperature and β is positive for all temperatures. Length parameters, London penetration depth, λ, and coherence length, ξ, are introduced as:

$$\lambda = \sqrt{\frac{mc^2\beta}{16\pi e^2|\alpha|}}$$

$$\xi = \frac{h}{2\pi\sqrt{2m|\alpha|}} \tag{9}$$

Ginzburg-Landau parameter, κ, is defined as the ratio of penetration depth and coherence length i.e. $\kappa=\lambda/\xi$. A length scale l is chosen and dimensionless length and time coordinates, order parameter ψ and magnetic potential A according to:

$$x \longrightarrow lx$$

$$\psi \longrightarrow \sqrt{\frac{|\alpha|}{\beta}}\psi$$

$$\boldsymbol{A} \longrightarrow \sqrt{\frac{8\pi|\alpha|^2 l^2}{\beta}}\boldsymbol{A} \tag{10}$$

$$\boldsymbol{B} \longrightarrow \sqrt{\frac{8\pi|\alpha|^2}{\beta}}\boldsymbol{B}$$

For the present work, length scale is chosen to be $l=\lambda$. In dimensionless form TDGL equations are given as:

$$\frac{\partial\psi}{\partial t} = \psi - |\psi|^2\psi - \left(\iota\frac{1}{\kappa}\boldsymbol{\nabla} + \boldsymbol{A}\right)^2\psi \tag{11}$$

$$\frac{\partial\boldsymbol{A}}{\partial t} = \boldsymbol{\nabla}\times(\boldsymbol{\nabla}\times\boldsymbol{A} - \boldsymbol{B}) + |\psi|^2\boldsymbol{A} + \frac{\iota}{2}\frac{1}{\kappa}(\psi^*\boldsymbol{\nabla}\psi - \psi\boldsymbol{\nabla}\psi^*) \tag{12}$$

with boundary conditions:

$$\left(\iota\frac{1}{\kappa}\boldsymbol{\nabla} + \boldsymbol{A}\right)\psi.\boldsymbol{n} = 0 \tag{13}$$

$$(\boldsymbol{\nabla}\times\boldsymbol{A})\times\boldsymbol{n} = \boldsymbol{B}\times\boldsymbol{n} \tag{14}$$

where $\boldsymbol{n}$ denotes perpendicular normal unit vector on the boundary and $\boldsymbol{B}$ denotes applied magnetic field. Equations (11), (12), (13) and (14) constitute the basis of numerical simulation of Abrikosov vortices and their dynamics for superconductor in the present work.

Energy density $H_{tot}=H_{tot}(x,y,z,t)$ in superconductor have three parts, magnetic energy density $H_{mag}=H_{mag}(x,y,z,t)$, superconducting energy density $H_{sup}=H_{sup}(x,y,z,t)$ and interaction energy density $H_{int}=H_{int}(x,y,z,t)$ given as;

$$H_{mag} = (B - \nabla \times A)^2 \tag{15}$$

$$H_{sup} = \frac{1}{\kappa^2}|\nabla\psi|^2 - |\psi|^2 + \frac{1}{2}|\psi|^4 \tag{16}$$

$$H_{int} = \frac{\iota}{\kappa}A\big((\nabla\psi)\psi^* - \psi(\nabla\psi^*)\big) + |A|^2|\psi|^2 \tag{17}$$

Total energy density is sum of these energy densities, $H_{tot} = H_{mag} + H_{sup} + H_{int}$, total energy can be calculated by integrating total energy density over the region Ω, $G_{tot} = \int H_{tot}(x,y,z,t)d\Omega$. Applied current is fixed in the direction perpendicular to the direction of magnetic field (i.e. in the plane of superconducting layer) and along one of the length directions (for this case x-axis). Therefore, we introduced an additional term J_x to x-component of vector potential A (i.e. A_x), as a dimensionless representation of current, which transforms to A_x+J_x.

3. RESULTS AND DISCUSSIONS

The schematic drawing of SF bilayer model is shown in figure 1 (not showing substrate, electrical contacts etc. for simplicity). Both layers are separated by an insulating (buffer) layer with thickness ξ, which inhibits electronic coupling. In our model, we focused on niobium (Nb) as the selected superconducting material with ξ=12 nm and λ=61 nm, working temperature of 6 K (T/T_c=0.674) with bulk upper critical magnetic field H_{c2}=7474 Oe [54, 55]. $CoFe_2O_4$ is chosen as the ferromagnetic material due to its extensive use in magnetic storage media and ability to withstand strong magnetic fields (high anisotropy constant). $CoFe_2O_4$ is known to have magnetic parameters, α_m=1, M_s=3.5×10^5 Am^{-1}, K_u=1×10^5 Jm^{-3} and A=7×10^{-12} Jm^{-1} [56]. Length and width of simulation area SC layer chosen to be 1000 nm (x-axis) × 1000 nm (y-axis) periodic along the direction of flow of current (x-axis) to form stripes, with 60 nm inter slab spacing (5ξ, sufficiently large to avoid any electric/magnetic coupling through an insulating vacuum). Single FM layer spreads under several SC stripes, therefore, relatively larger size of 2000 nm (x-axis) x 2000 nm (y-axis) of FM layer periodic in xy-plane was simulated. The thickness of SC layer was chosen to be 36 nm (z-axis), sufficiently thick to avoid dominance of surface effects while not being too thick to affect the strength of stray magnetic field from FM layer, while FM layer was chosen to be 36 nm (z-axis) thick for symmetry. Thickness of buffer layer was taken as 12 nm. Current density J_x was varied from 0 to 0.1 (which is significantly lower than our calculated critical current density ranging from 0.22 to 0.38 for external magnetic field range from 1000 Oe to 0 Oe) in reduced dimensions as the current wave. All calculation was performed by using a three-dimensional

coupled Ginzburg-Landau and Landau-Lifshitz-Gilbert equations using the code we have developed and reported earlier [50, 53, 57, 58].

Initially, the FM layer with random initial magnetic distribution was solved to minimize energy with uniaxial anisotropy and saturation magnetization pattern was obtained. Then a completely superconducting sample (i.e. $|\psi|^2=1$), with zero magnetic vector potential and zero J_x was subjected to a magnetic field pattern defined by stray field of FM layer with natural boundary conditions. Superconducting layer was relaxed to minimize Gibbs free energy, resulting in generation of vortex-antivortex (vortex with opposite spin) (V-AV) pairs and their rearrangement under domain centres of different types (upward and downward) of domains. The magnetic field strength of vortices in the SC layer was calculated to be less than 1% of the magnetic field strength of the FM layer, so was neglected. As system reached equilibrium state current wave was introduced to the sample. During increase and decrease of current density cycle, in the SC layer, V-AV pairs are generated and annihilated (and some enter and leave) continuously with the rate depending on the current density (or value of J_x) in the sample. After each cycle of current wave ($J_x = 0 \rightarrow 0.1 \rightarrow 0$) superconducting parameters e.g. carrier concentration ($|\psi|^2$), interaction energy (H_{int}), magnetic energy (H_{mag}), superconducting Energy (H_{sup}) and sample magnetization (M) were calculated. Application of external current to SC layer is particularly interesting as it drives V-AV in opposite direction due to Lorentz force. In other words, the current along V-AV pair would force vortex in one direction and antivortex to another causing a vortex pair-breaking mechanism. If the current is sufficient enough (for this case $I=0.06$) this Lorentz force can overcome domain wall barrier, resulting in the annihilation of V-AV pairs from the opposite side of the domain wall, this effect is discussed below in detail.

Micromagnetic simulations were initialized from a random distribution of magnetization, under a given external magnetic field with periodic boundary conditions for a finite size FM film with uniaxial anisotropy. External magnetic field was applied in the direction of magnetic domain orientation. As the domain structure was uniaxially anisotropic, therefore, in order to observe the maximum effect of external magnetic field, external magnetic field was selected parallel to domain orientation of ferromagnetic layer (i.e. normal to the film, along z-axis). In the condition of no applied magnetic field, the upward and downward magnetization covered equal sample areas and average sample magnetization was close to zero. But as magnetic field was increased, magnetization in the direction of the external magnetic field increased, as a result, vortex pattern in the SC layer under the FM layer changed accordingly. This whole effect is shown in figure 2 for a range of external magnetic fields for region of size 1000 nm x 1000 nm. The upward and downward magnetization directions are represented by purple and green colours while carrier concentration increases from zero (i.e. 0% of SC state) to 1 (i.e. 100% of SC state) represented by blue and red colours. Magnetic domain structure gradually changed from striped domains to bubble domains with increasing external magnetic field. So, the

magnetization structure in FM layer depends on the external magnetic field and as a result effects SC layer. In order to investigate the magnetic field experienced by SC layer, stray field was calculated outside the FM layer in the region of SC layer. Stray field plays a vital role in the nucleation of magnetic vortices (and antivortices) in SC layer, it reduces in intensity towards the uniform external magnetic field as the distance from the FM layer is increased. Therefore, it was necessary to keep SC layer close enough and sufficiently thin to experience stray field of FM layer and far enough to avoid current leakage between the layers.

SC layer was initially set at completely superconducting without any carrier loss (i.e. $|\psi|^2=1$) with zero magnetic vector potential (A), and natural boundary conditions on the boundaries perpendicular to current flow direction otherwise periodic, under an external magnetic field. The whole system was relaxed to minimize Gibbs free energy, resulting in entrance and rearrangement of vortices in superconductor. Magnetic domain structure for a range of external magnetic fields is shown in figure 2 with corresponding vortex structure before the introduction of any current pulse through the superconductor. It can clearly be seen that vortex structure in SC layer strongly depends on the magnetic configuration of ferromagnetic layer, FM layer is responsible for vortex pattern in SC layer in its vicinity.

Figure 3 shows the variation of interaction energy and carrier concentration with time at different values of current. Figure 3a,b,c represents spatial variation of interaction energy of the superconductor over magnetic domain cross-section (reference line figure 3g) with time for different values of current, where thin vertical lines in plot indicates approximate position of domain walls, reference line is shown as red line in carrier concentration plot in figure 3g, where arrows indicate domain walls and dot and cross symbols represent domain magnetization direction inward and outward respectively. It was observed that interaction energy is low at sites over domain wall contrary to those over the domain centres resulting in enhanced vortex mobility over the domain centres. Figure 3a, b are the overlaps of interaction energy with time, it can be seen that at lower current values vortices are pushed in one direction due to Lorentz force and antivortices to the other, but the force is not enough to overcome the energy barrier created by domain walls under the superconductor. It can be clearly seen that at current $J_x=0.06$ (figure 3c) there is a time variation in interaction energy shown by a spread in interaction energy spectrum, this is due to the fact that current has reached the threshold of formation and annihilation of V-AV pair at different types of domain walls (upward to downward domain switching and downward to upward domain switching). Vortices are formed at one type of domain wall and annihilated at the other. The same effect can also be seen in spatial plots of carrier concentration of the superconductor over magnetic domain cross-section with time for different values of current, at currents higher than $J_x=0.06$, time split in carrier concentration is observed indicating the dynamics of vortices over the domain centres, shown in figures 3f.

Figure 4 shows variation of carrier concentration, interaction energy, magnetic energy, superconducting energy and sample magnetization of SC layer before, during and after the introduction of current (arrows are time directional), for different magnetic field strengths. It was observed that carrier concentration of the sample was reduced by applying and removing the current peak. Similar reductions were observed for interaction energy, and magnetic energy, while superconducting energy and sample magnetization have shown an increase in their value. This change due to applied current pulse and the ability of the sample to retain a new state after the removal of the current pulse lead to the conclusion that such a system can work as an information storage device. It was observed that in such a hybrid system there can be multiple intermediate states of the sample in transit regime, with multiple energy minimization states. To investigate this effect further we applied periodic currents and calculated carrier concentrations after each current cycle. Figure 5a shows variation of carrier concentration of the sample over a number of cycles, it can clearly be observed that each peak representing zero current state, is at lower carrier concentration compared to the similar previous state. To our excitement, we observed various equilibrium states of SC layer each having lower carrier concentration than the previous one. In other words, SC layer was retaining its memory of the number of current pulses in carrier concentration (or resistivity) of the sample, which is one of the basic characteristics of memristors, as predicted by Chua *et. al.* in 1971 [39]. The initial state is not completely superconducting due to V-AV pair formation in the vicinity of FM layer. Figure 5b shows internediate states of carrier concentration in transit regime, after each pulse. It was also observed that this effect becomes smaller with the number of cycles and systemically reach zero variation. This type of device may have the ability to work as multi-bit storage devices contrary to single bit semiconductor registers.

Normally the vortices enter the sample from the edges but when FM layer is brought closer an additional magnetic field gradient is experienced by SC layer, that additional magnetic field generates V-AV pairs in addition to vortices entering from the sample boundaries (in the presence of external magnetic field). The stray magnetic field from FM layer is not strong enough to generate a larger number of V-AV pairs, so a lower density of vortices in SC layer appears in SC layer which avoids domain wall. Vortices arrange themselves under strong magnetic field positions i.e. domain centres. When current is introduced in the sample this passing current produces more V-AV pairs over domain walls which are pushed towards the opposite domain wall of a particular domain due to Lorentz force. When current is removed, these vortices settle down in the spaces between domain walls (i.e. under domain centres) with higher density. This high vortex density resulted in lower average carrier concentration and higher resistivity, which can be controlled by controlling height and width of current pulse. With every current cycle, this carrier concentration reduces and resistivity increases until it reaches its minimum state after a number of cycles and then varies randomly after reaching saturation value. The saturated device can be reset by decoupling SC and FM layers, which can be performed by a number of possible ways (e.g. destroying FM domain structure using current, using type-I SC material as a buffer layer which is

insulator above T_c). The behaviour of storage of information in resistivity of a material (or resistance of a device) is the fundamental characteristic (definition) of memristor [39]. Time-dependent resistivity presented here, whose value at a given time depends on the amount of charge passes through it (in the present state in the form of current pulses) is one of the definitions of a memristor [59, 60]. Therefore, we propose such a type of SF bilayer system to the scientific community for further investigation in order to fill in missing spaces in the fundamental electronic device, memristor. Moreover, superconducting memory is one of the voids in superconducting computing, the present work also proposes a multibit superconducting information storage device.

4. CONCLUSION

In this report, we investigated the possibility of using superconductor-ferromagnet bilayer with magnetostatic coupling as an information storage device. Coupled Landau-Lifshitz-Gilbert and Ginzburg-Landau equations were solved for ferromagnetic and superconducting layers respectively for three-dimensional geometries. Stray field by ferromagnetic layer was calculated in the region occupied by the superconducting layer. The effect of external magnetic field on ferromagnetic domain structure was studied along with resulting effect on superconductor film for a range of external magnetic field strengths. A time split in carrier concentration and interaction energy was observed near a threshold current ($J_x=0.06$), indicating continuous formation and annihilation of vortex-antivortex pairs on opposite domain walls. Carrier concentration, energy components and magnetization in superconductor layer were studied as a function of applied current in superconductor layer, showing a significant drop in carrier concentration after the current pulse along with significant changes in energy components and sample magnetizations. This indicates a strong dependence of carrier concentration/resistivity (and energy components) on the current pulse, storing its information. This variation in carrier concentration was observed systematically for a number of current pulses after which it varied randomly, these systematic states for several pulses indicate a possibility of such system to be used as a multibit storage device. This type of system can be a possible candidate for superconducting memory devices and missing circuit element memristor.

Acknowledgements

This work was supported by National Science Foundation of China grant numbers 11174030 and 11504020. Author H.M.J. acknowledges Higher Education Commission of Pakistan for the PhD scholarship.

References

1. Berk, N. and J. Schrieffer, *Effect of ferromagnetic spin correlations on superconductivity.* Physical Review Letters, 1966. **17**(8): p. 433.
2. Saxena, S., et al., *Superconductivity on the border of itinerant-electron ferromagnetism in UGe 2.* Nature, 2000. **406**(6796): p. 587.
3. Kim, K., et al., *Flux pinning with a magnetic nanorod array.* Applied Physics Letters, 2010. **97**(4): p. 042501.
4. Bartolomé, E., et al., *Hybrid YBa2Cu3O7 Superconducting–Ferromagnetic Nanocomposite Thin Films Prepared from Colloidal Chemical Solutions.* Advanced Electronic Materials, 2017. **3**(7): p. 1700037.
5. Hoffmann, A., et al., *Superconducting Vortex Pinning with Magnetic Dots: Does Size and Magnetic Configuration Matter?* Journal of Superconductivity and Novel Magnetism, 2012. **25**(7): p. 2187-2191.
6. Aladyshkin, A.Y., J. Fritzsche, and V. Moshchalkov, *Planar superconductor/ferromagnet hybrids: Anisotropy of resistivity induced by magnetic templates.* Applied physics letters, 2009. **94**(22): p. 222503.
7. Carneiro, G., *Simple model for tunable vortex pinning by a magnetic dipole.* Physica C: Superconductivity and its applications, 2006. **437**: p. 42-45.
8. Vlasko-Vlasov, V., et al., *Guiding superconducting vortices with magnetic domain walls.* Physical Review B, 2008. **77**(13): p. 134518.
9. Silhanek, A., et al., *Tunable pinning in superconducting films with magnetic microloops.* Applied physics letters, 2006. **89**(18): p. 182505.
10. Vodolazov, D.Y., et al., *Considerable enhancement of the critical current in a superconducting film by a magnetized magnetic strip.* Physical Review B, 2005. **72**(6): p. 064509.
11. Morelle, M. and V. Moshchalkov, *Enhanced critical currents through field compensation with magnetic strips.* Applied physics letters, 2006. **88**(17): p. 172507.
12. Belkin, A., et al., *Superconductor/ferromagnet bilayers: Influence of magnetic domain structure on vortex dynamics.* Physical Review B, 2008. **77**(18): p. 180506.
13. Belkin, A., et al., *Tunable transport in magnetically coupled MoGe/Permalloy hybrids.* Applied Physics Letters, 2008. **93**(7): p. 072510.
14. Vlasko-Vlasov, V., et al., *Soft magnetic lithography and giant magnetoresistance in superconducting/ferromagnetic hybrids.* Physical Review B, 2008. **78**(21): p. 214511.
15. Petrashov, V., et al., *Giant mutual proximity effects in ferromagnetic/superconducting nanostructures.* Physical review letters, 1999. **83**(16): p. 3281.
16. Mironov, S., A. Mel'nikov, and A. Buzdin, *Long-range inverse proximity effect in superconductor-ferromagnet structures.* arXiv preprint arXiv:1803.03926, 2018.
17. Bergeret, F., A. Volkov, and K. Efetov, *Long-range proximity effects in superconductor-ferromagnet structures.* Physical review letters, 2001. **86**(18): p. 4096.
18. Stahn, J., et al., *Magnetic proximity effect in perovskite superconductor/ferromagnet multilayers.* Physical Review B, 2005. **71**(14): p. 140509.
19. Machon, P., M. Eschrig, and W. Belzig, *Nonlocal thermoelectric effects and nonlocal Onsager relations in a three-terminal proximity-coupled superconductor-ferromagnet device.* Physical review letters, 2013. **110**(4): p. 047002.
20. Buzdin, A.I., *Proximity effects in superconductor-ferromagnet heterostructures.* Reviews of modern physics, 2005. **77**(3): p. 935.
21. Zhen, S., et al., *Proximity Effects of Superconductivity and Antiferromagnetism in a Nanowire.* Journal of Superconductivity and Novel Magnetism, 2019: p. 1-5.
22. Lazar, L., et al., *Superconductor/ferromagnet proximity effect in Fe/Pb/Fe trilayers.* Physical Review B, 2000. **61**(5): p. 3711.
23. Volkov, A., F. Bergeret, and K. Efetov, *Spin polarization and orbital effects in superconductor-ferromagnet structures.* arXiv preprint arXiv:1901.04446, 2019.

24. Buzdin, A.I. and A. Mel'nikov, *Domain wall superconductivity in ferromagnetic superconductors.* Physical Review B, 2003. **67**(2): p. 020503.
25. Gillijns, W., et al., *Domain-wall guided nucleation of superconductivity in hybrid ferromagnet-superconductor-ferromagnet layered structures.* Physical review letters, 2005. **95**(22): p. 227003.
26. Yang, Z., et al., *Domain-wall superconductivity in superconductor–ferromagnet hybrids.* Nature materials, 2004. **3**(11): p. 793.
27. Aikebaier, F., P. Virtanen, and T. Heikkilä, *Superconductivity near a magnetic domain wall.* Physical Review B, 2019. **99**(10): p. 104504.
28. Houzet, M. and A.I. Buzdin, *Theory of domain-wall superconductivity in superconductor/ferromagnet bilayers.* Physical Review B, 2006. **74**(21): p. 214507.
29. Bergeret, F., A. Volkov, and K. Efetov, *Induced ferromagnetism due to superconductivity in superconductor-ferromagnet structures.* Physical Review B, 2004. **69**(17): p. 174504.
30. Wang, X., et al., *Spintronic memristor through spin-torque-induced magnetization motion.* IEEE electron device letters, 2009. **30**(3): p. 294-297.
31. Córdoba, R., et al., *Magnetic field-induced dissipation-free state in superconducting nanostructures.* Nature communications, 2013. **4**: p. 1437.
32. Li, J., et al., *Topological superconductivity induced by ferromagnetic metal chains.* Physical Review B, 2014. **90**(23): p. 235433.
33. Gu, J., et al., *Magnetization-Orientation Dependence of the Superconducting Transition Temperature in the Ferromagnet-Superconductor-Ferromagnet System: C u N i/N b/C u N i.* Physical review letters, 2002. **89**(26): p. 267001.
34. Mühge, T., et al., *Possible origin for oscillatory superconducting transition temperature in superconductor/ferromagnet multilayers.* Physical review letters, 1996. **77**(9): p. 1857.
35. Buzdin, A.I. and M.Y. Kupriyanov, *Transition temperature of a superconductor-ferromagnet superlattice.* JETP Lett, 1990. **52**(9).
36. Leksin, P., et al., *Evidence for triplet superconductivity in a superconductor-ferromagnet spin valve.* Physical review letters, 2012. **109**(5): p. 057005.
37. Kalcheim, Y., et al., *Long-range proximity effect in La 2/3 Ca 1/3 MnO 3/(100) YBa 2 Cu 3 O 7–δ ferromagnet/superconductor bilayers: evidence for induced triplet superconductivity in the ferromagnet.* Physical Review B, 2011. **83**(6): p. 064510.
38. Bergeret, F., A.F. Volkov, and K.B. Efetov, *Odd triplet superconductivity and related phenomena in superconductor-ferromagnet structures.* Reviews of modern physics, 2005. **77**(4): p. 1321.
39. Chua, L., *Memristor-the missing circuit element.* IEEE Transactions on circuit theory, 1971. **18**(5): p. 507-519.
40. Campbell, K.A., *Self-directed channel memristor for high temperature operation.* Microelectronics Journal, 2017. **59**: p. 10-14.
41. Williams, R.S., *How we found the missing memristor.* IEEE spectrum, 2008. **45**(12).
42. Xiao, Z. and J. Huang, *Energy‐efficient hybrid perovskite memristors and synaptic devices.* Advanced Electronic Materials, 2016. **2**(7): p. 1600100.
43. Bessonov, A.A., et al., *Layered memristive and memcapacitive switches for printable electronics.* Nature materials, 2015. **14**(2): p. 199-204.
44. Chanthbouala, A., et al., *A ferroelectric memristor.* Nature materials, 2012. **11**(10): p. 860-864.
45. Ageev, O., et al., *Memristor effect on bundles of vertically aligned carbon nanotubes tested by scanning tunnel microscopy.* Technical Physics, 2013. **58**(12).
46. Wang, L., et al., *Rectification‐Regulated Memristive Characteristics in Electron‐Type CuPc‐Based Element for Electrical Synapse.* Advanced Electronic Materials, 2017. **3**(7): p. 1700063.
47. Liu, G., et al., *Organic biomimicking memristor for information storage and processing applications.* Advanced Electronic Materials, 2016. **2**(2): p. 1500298.

48. Yang, J.M., et al., *1D Hexagonal HC (NH2) 2PbI3 for Multilevel Resistive Switching Nonvolatile Memory.* Advanced Electronic Materials, 2018. **4**(9): p. 1800190.
49. Zhang, J. and L. Chen, *Phase-field microelasticity theory and micromagnetic simulations of domain structures in giant magnetostrictive materials.* Acta Materialia, 2005. **53**(9): p. 2845-2855.
50. Huang, H., et al., *Simulation of multilevel cell spin transfer switching in a full-Heusler alloy spin-valve nanopillar.* Applied physics letters, 2013. **102**(4): p. 042405.
51. GoR'Kov, L.P. and G.M. Eliashberg, *Generalization of the Ginzburg-Landau equations for non-stationary problems in the case of alloys with paramagnetic impurities.* Soviet Journal of Experimental and Theoretical Physics, 1968. **27**: p. 328.
52. Du, Q., M.D. Gunzburger, and J.S. Peterson, *Computational simulation of type-II superconductivity including pinning phenomena.* Physical Review B, 1995. **51**(22): p. 16194.
53. Jafri, H.M., et al., *Numerical simulation of vortex dynamics in type-II superconductors in oscillating magnetic field using time-dependent Ginzburg–Landau equations.* Journal of Physics: Condensed Matter, 2017. **29**(50): p. 505701.
54. Bobba, F., et al., *Vortex-antivortex coexistence in Nb-based superconductor/ferromagnet heterostructures.* Physical Review B, 2014. **89**(21): p. 214502.
55. Iavarone, M., et al., *Imaging the spontaneous formation of vortex-antivortex pairs in planar superconductor/ferromagnet hybrid structures.* Physical Review B, 2011. **84**(2): p. 024506.
56. Hu, J.-M. and C. Nan, *Electric-field-induced magnetic easy-axis reorientation in ferromagnetic/ferroelectric layered heterostructures.* Physical Review B, 2009. **80**(22): p. 224416.
57. Zhao, C., et al., *Micromagnetic simulation of boundary pinning effects on spectra in a point-contact spin torque oscillator.* IEEE Magnetics Letters, 2017. **PP**(99): p. 1-1.
58. Jafri, H.M., et al., *Numerical Simulation of Phase Transitions in Type-II Annular Superconductor Using Time-dependent Ginzburg-Landau Equations.* Journal of Superconductivity and Novel Magnetism, 2018. **31**(11): p. 3445-3451.
59. Strukov, D.B., et al., *The missing memristor found.* nature, 2008. **453**(7191): p. 80.
60. Joglekar, Y.N. and S.J. Wolf, *The elusive memristor: properties of basic electrical circuits.* European Journal of Physics, 2009. **30**(4): p. 661.

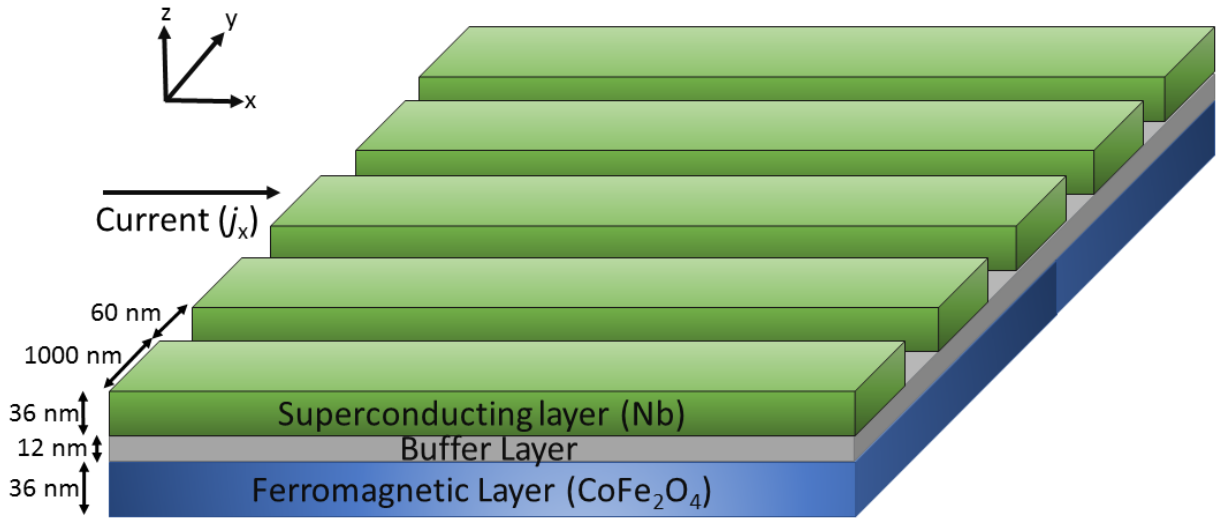

Figure 1. Schematic diagram of superconductor-ferromagnet bilayer system (not to scale) with 36 nm thick ferromagnetic film periodic in xy-plane, 36 nm thick and 1000 nm wide superconducting stripes separated by 60 nm, periodic along the x-axis.

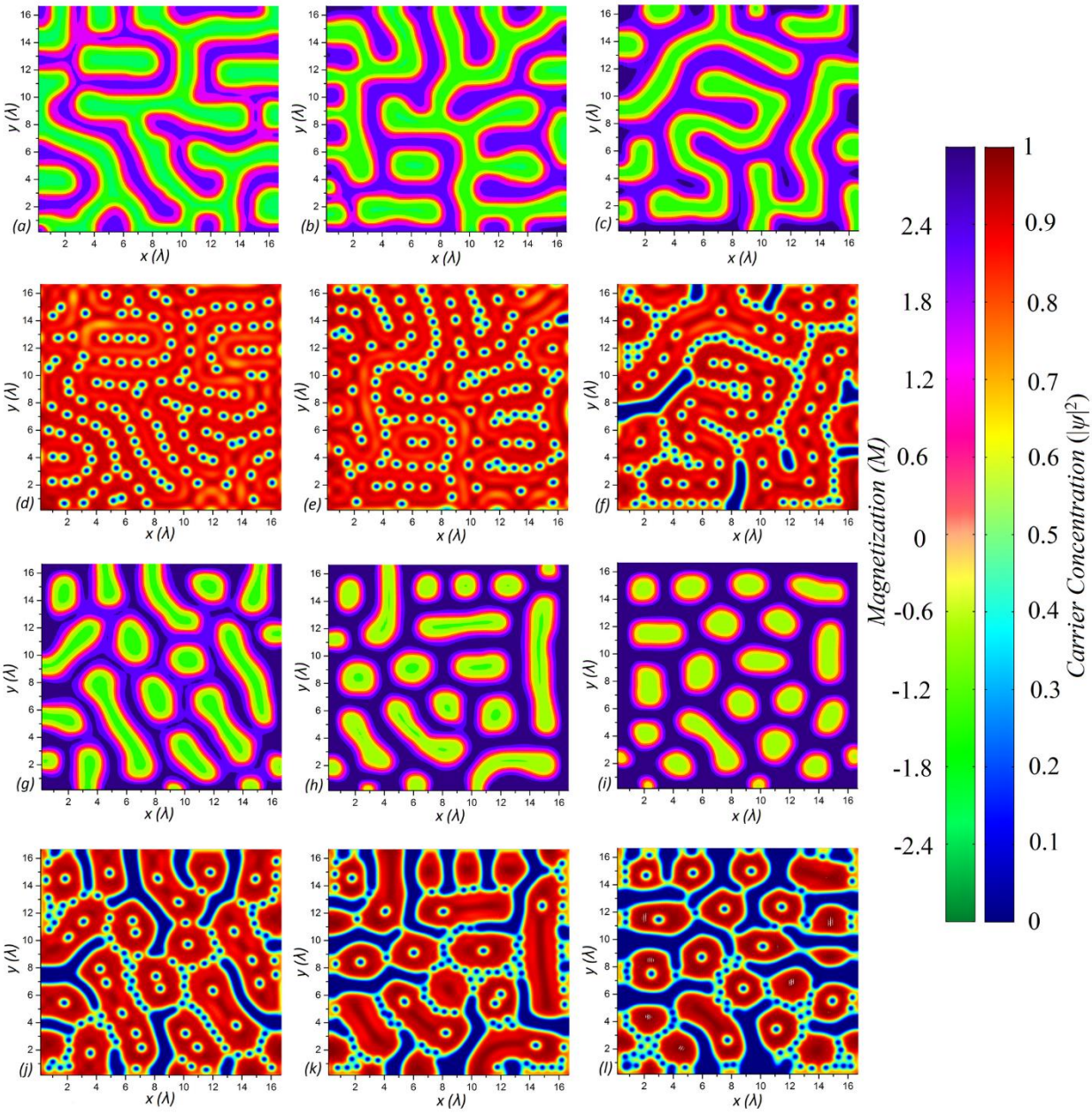

Figure 2. Magnetic domain structures (a,b,c,g,h,i) and corresponding vortex (antivortex) geometries (d,e,f,j,k,l) of cross-section, for bilayer system under H_{ext} = 0 Oe, 500 Oe, 1000 Oe, 1500 Oe, 1500 Oe, 2000 Oe and 2500 Oe respectively, size 1000 nm x 1000 nm for both layers and J_x=0, showing strong dependence of vortex (antivortex) geometry on magnetic domain structure.

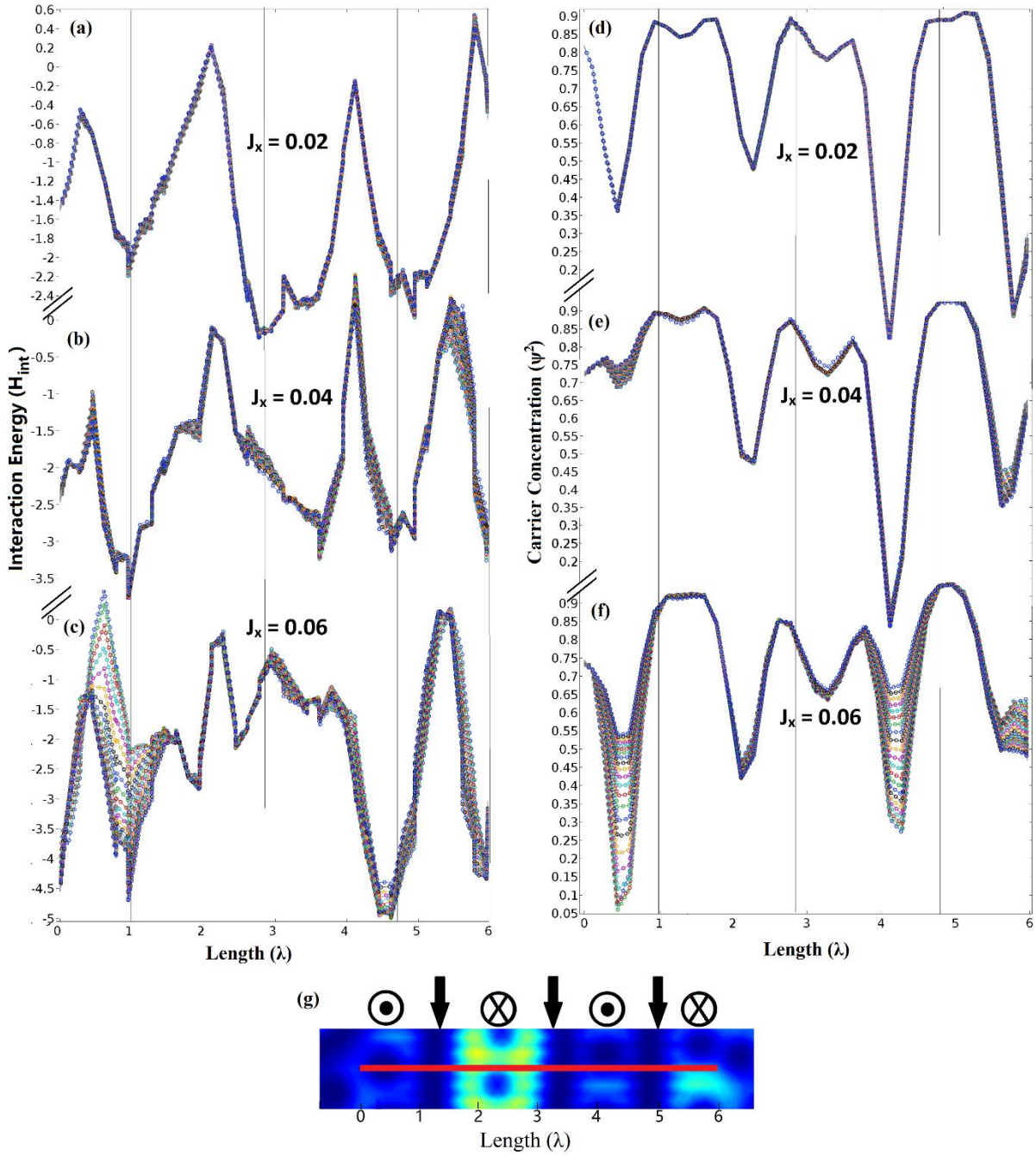

Figure 3. Temporal splitting of (a,b,c) interaction energy (H_{int}) and (d,e,f) carrier concentration ($|\psi|^2$) of superconductor layer under reference line (g). temporal splitting of H_{int} and $|\psi|^2$ observed at J_x=*0.02,0.04,0.06* and H_{ext}=*0 Oe*. (Grey vertical lines in plot indicate domain wall position), (g) represents the reference red line used for the above plots with arrows indicating the domain wall while dot and cross representing outward and inward domain centres. A wide split in time can be clearly observed at J_x=0.6 indicating continuous formation/annihilation of vortex-antivortex pairs (i.e. Lorentz force overcomes domain wall barrier).

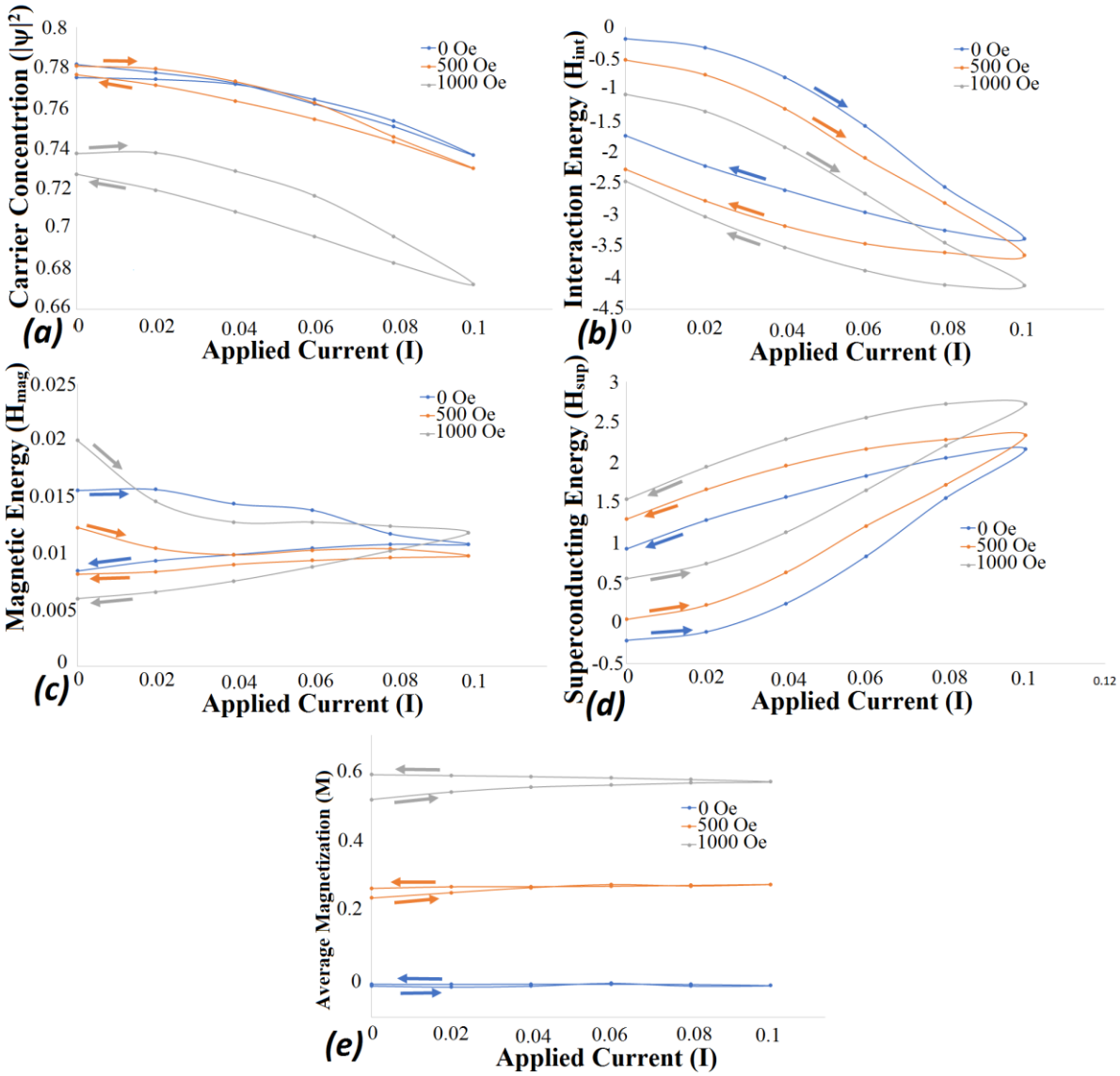

Figure 4. Variation of (a) carrier concentration, (b) interaction Energy, (c) magnetic energy, (d) superconducting energy and (e) average magnetization of superconducting layer for increasing and decreasing parts of current pulse at H_{ext}=*0 Oe, 500 Oe, 1000 Oe*, showing the dependence of state variables in current pulse (values of state variables can be clearly seen to have changed after a current pulse). Arrows are time directional.

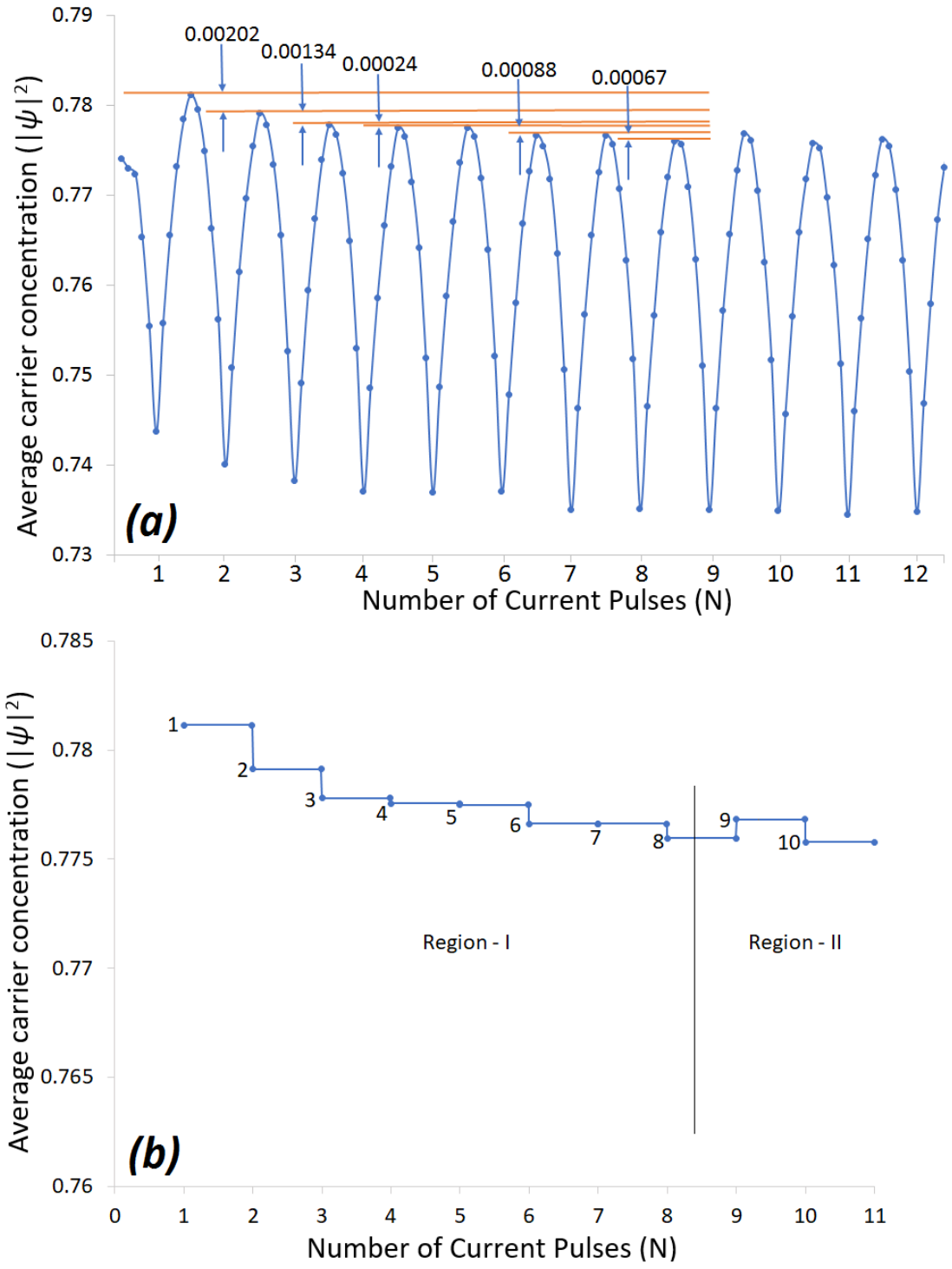

Figure 5. Temporal plots of carrier concentration for successive current pulses, (a) carrier concentration variation with current pule and (b) equilibrium states of carrier concentration after each pulse. Several carrier concentrations (or resistivity) states were observed before saturation takes place.